HHS Public Access

Author manuscript

Curr Biol. Author manuscript; available in PMC 2018 May 22.

Published in final edited form as:

Curr Biol. 2017 May 22; 27(10): 1413–1424.e4. doi:10.1016/j.cub.2017.03.077.

Theta Oscillations During Active Sleep Synchronize The Developing Rubro-Hippocampal Sensorimotor Network

Carlos Del Rio-Bermudez[1,4], **Jangjin Kim**[1], **Greta Sokoloff**[1,4], and **Mark S. Blumberg**[1,2,3,4,5]

[1]Department of Psychological & Brain Sciences, University of Iowa, Iowa City, IA 52242, USA

[2]Interdisciplinary Graduate Program in Neuroscience, University of Iowa, Iowa City, IA 52245, USA

[3]Department of Biology, University of Iowa, Iowa City, IA, 52242 USA

[4]DeLTA Center, University of Iowa, Iowa City, IA 52242 USA

Summary

Neuronal oscillations comprise a fundamental mechanism by which distant neural structures establish and express functional connectivity. Long-range functional connectivity between the hippocampus and other forebrain structures is enabled by theta oscillations. Here we show for the first time that the infant rat red nucleus (RN)—a brainstem sensorimotor structure— exhibits theta (4-7 Hz) oscillations restricted primarily to periods of active (REM) sleep. At postnatal day (P) 8, theta is expressed as brief bursts immediately following myoclonic twitches; by P12, theta oscillations are expressed continuously across bouts of active sleep. Simultaneous recordings from the hippocampus and RN at P12 show that theta oscillations in both structures are coherent, co-modulated, and mutually interactive during active sleep. Critically, at P12, inactivation of the medial septum eliminates theta in both structures. The developmental emergence of theta-dependent functional coupling between the hippocampus and RN parallels that between the hippocampus and prefrontal cortex. Accordingly, disruptions in the early expression of theta could underlie the cognitive and sensorimotor deficits associated with neurodevelopmental disorders such as autism and schizophrenia.

Keywords

neural oscillations; functional connectivity; development; REM sleep; local field potential; hippocampus; neurodevelopmental disorder

[5]Lead Contact: Mark S. Blumberg (mark-blumberg@uiowa.edu)

Author Contributions: C.D.R-B., M.S.B., and G.S. designed the experiments; C.D.R-B. collected the data; C.D.R-B., and J.K. analyzed the data; C.D.R-B., J.K., and M.S.B. wrote the paper.

Introduction

Sleep is the predominant behavioral state in early development [1–4]. Of the two primary sub-states of sleep, active sleep (AS, or REM sleep) occurs at its highest rates in the perinatal period and has long been considered a critical contributor to early brain development [4,5]. In addition, myoclonic twitching is a prominent phasic component of AS that triggers patterned neural activity throughout the neuraxis and, by doing so, can contribute to the experience-dependent development of sensorimotor networks [6–9].

We recently showed that the newborn red nucleus (RN) is an important site for sensorimotor integration [10]. Specifically, in week-old rats, the RN is not only involved in the generation of wake movements and AS-related twitching, but also processes sensory feedback from moving limbs in a somatotopic fashion. Importantly, the RN is functionally connected with many other sensorimotor structures, including the cerebellum [11,12], sensorimotor cortex [13], and hippocampus [14–16]. Although the hippocampus is most typically associated with spatial memory and navigation [17], it has also long been considered a sensorimotor structure [18,19]. According to the sensorimotor integration model of hippocampal function, the hippocampus interacts with the RN in a bidirectional manner to enable sensorimotor integration during motor performance [14,20]. The neural mechanisms that establish and maintain this long-range connectivity between hippocampus and RN have not been elucidated.

As demonstrated primarily in the adult [21–23] and infant [24–27] forebrain, long-range functional connectivity is maintained via synchronized neural oscillations, particularly at low frequencies including theta (4-10 Hz). In adults, oscillations in the theta band support functional connectivity in the hippocampus and associated networks during sensorimotor processing in humans [28] and rats [29]. Here we address the hypothesis that the infant hippocampus establishes long-range functional connectivity with the RN through synchronized theta oscillations. We record extracellular activity in P8 and P12 rats cycling freely between sleep and wakefulness; we chose these ages because they mark an abrupt transition in the development of hippocampal theta [30] as well as neural activity in the RN and associated structures [12]. We demonstrate for the first time that the RN exhibits robust theta activity during AS. Moreover, by P12, AS-related theta oscillations in the hippocampus and RN are coherent, comodulated, and mutually interactive. Finally, pharmacological inactivation of the medial septum (MS), an established generator of hippocampal theta, blocks AS- but not twitch-related theta in both the hippocampus and RN. These findings highlight the importance of behavioral state for the differential expression of functional connectivity in the developing nervous system. They also lay a foundation for understanding how neural oscillations contribute to the emergence of long-range functional connectivity linking cortical and brainstem networks.

Results

The infant RN exhibits state- and twitch-dependent theta oscillations

We first characterized developmental patterns of oscillatory activity in the RN using data from a previous study [12]. At P8 (n = 11), the local field potential (LFP) in the RN

exhibited short, discontinuous bursts of oscillatory activity (Figure 1A). These bursts occurred predominantly at theta frequency (4-7 Hz) and within periods of AS. In contrast, theta activity at P12 (n = 11) was continuous during periods of AS (Figure 1B). This rapid developmental transition from discontinuous to continuous oscillatory activity in the RN is similar to that observed in forebrain areas such as prefrontal cortex [24], sensorimotor cortex [31], and hippocampus [24,30]. Quantitative analyses of theta power revealed a significant main effect of Behavioral State ($F_{(2, 40)} = 4.9$, $p < 0.02$) as well as an Age × Behavioral State interaction ($F_{(2, 40)} = 14.6$, $p < 0.001$); theta power at P12 was significantly higher during AS in relation to the other behavioral states (post hoc pairwise comparisons, ps < 0.002; Figure 1C, D).

Sensory feedback (i.e., reafference) from myoclonic twitches is a potent driver of RN activity at P8 and P12 [10,12]. Thus, we next asked whether the brief theta oscillations observed during AS at P8 were attributable to twitch-related reafference. Individual twitch-triggered spectrograms and LFP waveforms of theta activity, pooled across all pups (n = 11), indicate that twitch-related reafference triggered brief theta oscillations ($p < .01$; Figure 2A). Surprisingly, at P12 and against a background of continuous theta oscillations (n = 11), twitch-related reafference continued to trigger increased theta power ($p < .01$; Figure 2B). This transition between P8 and P12 from brief, twitch-related theta bursts to continuous, AS-related oscillations in the RN mirrors previous findings in the hippocampus [30].

Theta oscillations in the hippocampus and RN are tightly coupled during AS at P12

We next asked whether the continuous theta oscillations in the hippocampus and RN, first observed at P12, are temporally coupled, thus indicating functional connectivity between these two structures. To address this question, we performed simultaneous extracellular recordings in the RN and hippocampal CA1 (n = 19; Figure 3A). As expected, continuous theta oscillations in the hippocampus and RN were most prominently expressed during AS (Figure 3B). Theta power was higher for periods of AS in both the hippocampus (Figure 3C, $F_{(1.4,25.9)} = 31.3$, $p < 0.001$, correction: Greenhouse-Geisser) and RN (Figure 3D; $F_{(1.4,26.1)} = 19.8$, $p < 0.001$, correction: Greenhouse-Geisser) in relation to active wake (AW) and behavioral quiescence (BQ; post hoc pairwise comparisons, ps < 0.001).

It should be noted that the theta-frequency peak observed here at P12 (5 Hz) is lower than that reported in the hippocampus of adult rats during AS (typically 8 Hz; Montgomery et al., 2008). The frequency peak found here at P12 is consistent with the finding of a progressive increase in theta frequency across age from ~5.5 Hz at P16 to ~7.5 Hz by P28 [33].

We next assessed the coherence of hippocampal and RN theta oscillations across the three behavioral states (Figure 4A). Coherence spectra revealed that coupling in the theta-frequency range was significantly greater during AS (Figure 4B; $F_{(2,36)} = 47.2$, $p < 0.001$) than during AW or BQ (ps < 0.001). To characterize the strength and directionality of information flow between the hippocampus and RN during AS, we next performed Granger causality analysis [34,35] (Figure 4C). This analysis was performed on LFP pairs from all 19 pups, from which we identified 9 pups that exhibited (i) significant Granger values (ps < 0.01) and (ii) clear Granger value peaks within theta frequency. From these pups, the average pattern comprised a substantial hippocampus→RN peak and a smaller RN

hippocampal peak. These results are consistent with the sensorimotor integration model of hippocampal function [14,20], which posits bidirectional communication between the hippocampus and RN.

Having established functional connectivity in the theta band between the hippocampus and RN, we next assessed whether theta oscillations are temporally associated with spiking activity in the two structures. Hippocampal spiking activity was highly coherent with hippocampal LFP in the theta-frequency range during AS ($F_{(1.1,39.4)} = 17.2$, $p < 0.004$, correction: Greenhouse-Geisser) as compared with AW and BQ (post hoc pairwise comparisons, ps < 0.004; Figure S1A). In contrast, theta-related spike-LFP coherence in the RN was negligible (Figure S1B). Visual examination of the RN data, however, suggested that spiking activity increases substantially during periods of increased theta amplitude (e.g., see Figure S2B). Therefore, we next examined the temporal fluctuations in theta amplitude before testing the hypothesis that spike-LFP coherence in the RN is enhanced during periods of high-amplitude theta.

Comodulation of theta amplitude in the hippocampus and RN at P12

We defined high-amplitude theta as continuous theta oscillations with at least three cycles that exceeded the baseline amplitude by 1.5 SDs; all other periods were designated as low-amplitude theta (Figure 5A). As expected, this method yielded two distinct categories of AS-related theta in the hippocampus ($F_{(1,18)} = 32.1$, $p < 0.001$) and RN ($F_{(1,18)} = 84.7$, $p < 0.001$; Figure 5B). High-amplitude theta during AS was often closely associated with periods of abundant myoclonic twitching (Figure 5A); indeed, rates of twitching in the forelimb were significantly higher during periods of high-amplitude theta in both the hippocampus ($F_{(1,18)} = 16.5$, $p < 0.002$) and RN ($F_{(1,18)} = 26.2$, $p < 0.001$; Figure 5C). Cross-correlations between theta-filtered LFPs in the hippocampus and RN during AS indicated robust synchrony and coherent amplitude modulation (i.e., comodulation; Figure 5D, left; mean lag for pooled data: 10 ± 9 ms); cross-correlations coefficients were significantly higher in relation to shuffled data ($t_{(18)} = 10.1$, $p < 0.001$; Figure 5D, right).

Theta oscillations modulate spiking activity in the hippocampus and RN at P12

Having characterized fluctuations in theta amplitude across AS, we next returned to the hypothesis that spike-LFP coherence is specifically enhanced during periods of high-amplitude theta. To test this hypothesis, we produced spike-LFP coherence spectra restricted to periods of high-amplitude theta and selected those units showing clear peaks within the theta-frequency range (see Methods). For these pairs, and in comparison to entire bouts of AS, spike-LFP coherence was significantly greater during periods of high-amplitude theta in the hippocampus ($F_{(1,23)} = 10.8$, $p < 0.004$; Figure 5E) and RN ($F_{(1,23)} = 29.5$, $p < 0.001$; Figure 5F).

In addition to spike-LFP coherence, hippocampal and RN units were phase-locked to local theta oscillations during periods of high-amplitude theta. Examples of phase-locked spiking activity are shown for the hippocampus (Figure 5G, left) and RN (Figure 5H, left). In total, significant phase-locking was found in 79% of the hippocampal neurons and 61% of the RN neurons (ps < 0.01). Moreover, phase locking was significantly higher during periods of

high-amplitude theta in both the hippocampus ($F_{(1,25)} = 9.8$, $p < 0.005$, Figure 5G, right) and RN ($F_{(1,35)} = 14.9$, $p < 0.001$; Figure 5H, right). These results suggest that theta oscillations in the developing hippocampus and RN modulate neuronal activity during AS, especially during periods of high-amplitude theta.

Spike-LFP coherence and phase locking within the RN suggest that theta oscillations are locally expressed rather than being volume conducted from a nearby structure. We further addressed this issue of local generation in a subset of P12 subjects (n = 5) by retracting the electrode to locations dorsal to the RN and performing additional recordings (Figure S2A). As shown for a representative subject (Figure S2B), theta power during AS was equally high in the two sites within the RN—where spiking activity was also present—and decreased at sites approximately 2 mm dorsal to the RN. This pattern of decrease in theta power was found in the theta ratios averaged across all five subjects (Figure S2C). Interestingly, the retention of high theta ratios in the region immediately dorsal to the RN could reflect RN-like activity in nearby premotor nuclei within the so-called mesodienchaphalic junction [36].

Inactivation of the medial septum blocks theta in the hippocampus and RN at P12

The findings presented thus far suggest that theta oscillations in the hippocampus and RN share a common neural generator. The medial septal area, including medial septum (MS) and diagonal band of Broca (DBB), is known to generate hippocampal theta in adult [37] and neonatal [24] rats. To determine whether it also generates theta in the RN, we compared hippocampal and RN activity at P12 before and after pharmacological inactivation of the MS (Figure 6A,B). These inactivations were performed in a subset of the subjects described above (n = 6 in each group) by infusing 0.1 μl of the $GABA_A$ receptor agonist muscimol (1.6 mM) or saline [38].

The LFPs and time-frequency spectrograms for one representative subject are shown in Figure 6C; in both the hippocampus and RN, theta oscillations during AS were markedly reduced after MS inactivation. These reductions are equally clear in the averaged power spectra in Figure 6D. With respect to theta power across the two structures, there was a significant main effect of Pre/Post (Hipp: $F_{(1,10)} = 9.3$, $p < 0.02$; RN: $F_{(1,10)} = 9.9$, $p = 0.01$) as well as a significant Group × Pre/Post interaction (Hipp: $F_{(1,10)} = 13.4$, $p < 0.005$; RN: $F_{(1,10)} = 8.7$, $p < 0.02$). Post hoc tests revealed significant decreases in theta power after MS inactivation for the hippocampus ($p < 0.02$; Figure 6D, top) and RN ($p = 0.01$; Figure 6D, bottom). Importantly, MS inactivation had no effect on the expression of AS or twitching (Table S1). Thus, the MS specifically modulates the expression of AS-related theta in both the hippocampus and RN without affecting the expression of sleep or twitching.

In addition to inputs from the forebrain, the RN receives a prominent input from the deep cerebellar nuclei (DCN) [11,39]. In a previous study that used similar methods in P12 rats (Figure S3A), we found that inactivation of the DCN reduced firing rates in the RN during AS by 40-50% [12]. We returned to these data to ask whether DCN inactivation had any effect on the expression of theta in the RN. We found that it did not (Figure S3B), thus providing further evidence that RN theta is specifically tied to the septo-hippocampal system.

Finally, spiking activity in both the hippocampus and RN [10,12,30] increases in response to twitching; in the hippocampus, twitch-related reafference is conveyed from the sensorimotor cortex [40]. This raises the possibility that twitch-triggered activation of theta bursts within the hippocampus and RN occur independently of septal influence. Indeed, inactivation of the MS at P12 blocked AS-related—but not twitch-related—theta in both the hippocampus and RN (all $p < 0.05$; Figure 7). Moreover, in the absence of septal input, twitch-triggered theta activity at P12 now mirrored the discontinuous theta-burst pattern observed here at P8 in the RN (see Figure 2A) and previously in the hippocampus [30].

Discussion

We have discovered in infant rats the presence of continuous theta oscillations in the RN, a premotor brainstem structure that plays an outsized role in controlling newborn behavior [10,41]. These theta oscillations emerged rapidly toward the end of the second postnatal week and were expressed predominantly during AS. By recording simultaneously from the RN and hippocampus at P12, we found that theta in the two structures was coherent and comodulated during AS, indicating close functional and state-dependent coupling between them. Finally, by inactivating the MS—a structure k nown to generate hippocampal theta—we found that theta is lost in both the hippocampus and RN. Although it has been proposed that theta oscillations in the hippocampus contribute to its functional connectivity with brainstem motor nuclei [20], the possibility of oscillatory coupling among these structures had not been considered.

The transition from discontinuous to continuous oscillatory activity

During AS, theta oscillations in the RN are expressed at P8 as discontinuous bursts and transition to continuous oscillations by P12; this transition from discontinuous to continuous theta is identical to that observed in the hippocampus [30]. Similar oscillatory transitions have been reported in the rat cerebral cortex at the beginning of the second postnatal week [7,24,27,30,31] and in human infants toward the end of the third trimester [27,42,43]. In rats, these transitions coincide with abrupt increases in single-unit firing rates in the RN [12], cerebellum [12,44], sensorimotor cortex [31], and hippocampus [30]. Moreover, the rapidity with which these transitions occur suggest that these ages define a sensitive period for brain development [44].

The emergence of hippocampal theta bursts at P8 [30] coincides with the rapid proliferation of perisomatic interneuronal synapses [45] and the emergence of parvalbumin-immunoreactive GABAergic neurons in the MS and hippocampus [46,47]; both contribute to theta production [48,49]. Like the hippocampus, the rodent RN contains a well-characterized subpopulation of GABAergic interneurons, including parvalbumin-immunoreactive cells [50,51]. In addition, the density of GABAergic receptors in the rat RN peaks around P10 [52], just before the emergence of continuous theta. The similarities in the developmental timing of theta in the RN and hippocampus, as well as similarities in the emergence of GABAergic networks, suggest that theta in both structures is generated through similar mechanisms.

As illustrated in Figure S4, continuous theta in the RN could arise through a number of different pathways. Specifically, RN theta could arise independently of the hippocampus through direct or indirect input from the septal area, including the MS and the DBB [53], or through an indirect projections from the hippocampus, perhaps through the zona incerta [53,54] or the lateral septum and hypothalamus [53,55].

Reafference from twitches triggers a third type of theta activity

At P8, discontinuous theta bursts in the RN were predominantly expressed immediately after forelimb twitches, suggesting reafferent activation. Bursts of oscillatory activity can contribute to a variety of developmental processes, including synapse formation, cell differentiation and migration [27], and map formation and refinement [25]. Importantly, the close temporal association between twitching and brief bursts of cortical [7,31] and hippocampal [30] activity inspired the hypothesis that twitch-related reafference contributes to the development of these forebrain networks [6,7,9]. The present findings extend these ideas to brainstem structures like the RN [10]. To the extent that increases in LFP power reflect enhanced neuronal synchrony [56], twitch-triggered increases in theta power may reflect greater network synchronization in the rubro-hippocampal system.

In the adult hippocampus, two types of theta oscillations have been identified, based in part on their behavioral correlates [57]: Type 1 or movement-related, theta, and type 2 or immobility-related theta. Moreover, whereas type 1 theta occurs during periods of “phasic AS” (defined by the presence of phasic events, including twitches), and type 2 theta occurs during “tonic AS” [58]. At P12 during AS, hippocampal theta exhibited characteristics that correspond with types 1 and 2, and inactivation of the MS suppressed both of them, as occurs in adults [59]. Strikingly, we found the same pattern of results in the P12 RN.

During AS, Type 1 theta is identified only with *periods* surrounding phasic activity and has not been specifically associated with reafference from twitches. In contrast, as noted above, inactivation of the MS at P12 suppressed both types of theta while sparing the expression of twitch-triggered theta bursts; this suggests that reafferent theta is conveyed via non-septal pathways (see Figure S4). This finding raises the possibility that twitch-reafferent theta in adults is present but masked, as previously proposed in relation to twitch-reafferent spindle-burst activity in sensorimotor cortex [60]. Accordingly, we propose that twitch-reafferent theta constitutes a distinct—type 3—category of theta. Th e pathways conveying twitch-related reafference to the RN likely bypass the cerebellum [12] and involve direct spinorubral projections [61]; on the other hand, the pathway to the hippocampus likely passes first through somatosensory cortex [40].

The rubro-hippocampal network and its role in sensorimotor integration

In adults, functional connectivity between the hippocampus and RN is thought to enable motor behavior that adjusts adaptively to sensory input [14,20]. For example, both the hippocampus and RN are necessary for the acquisition and expression of trace eyeblink conditioning [16,62], and theta oscillations appear important for synchronizing the hippocampus and cerebellum to enhance this learning [63]; this opens the possibility that theta oscillations in the RN also participate in this system-wide synchronization within

learning contexts. In addition, the role of hippocampal theta in modulating locomotor speed in mice [64] may be mediated by subcortical premotor structures such as the RN. Theta-dependent functional connectivity could also contribute to the acquisition and consolidation of skilled forelimb movements, which are highly dependent on the RN [65].

Functional connectivity in developing networks: Beyond the "resting state"

Although AS is a relatively prominent behavioral state in early infancy [1–4], investigations of functional connectivity in infants have largely focused on the so-called "resting state," on periods of slow-wave sleep, or under anesthetic conditions that suppress normal sleep-wake cycles [66]. Given the hypothesized role of AS in brain development [1,4–6], one might expect network interactions to be very different during this sleep state; indeed, in adults, AS specifically enhances theta-dependent synchrony in hippocampal networks [32,67] and, moreover, AS-related theta appears to be causally related to hippocampal-dependent memory consolidation [68]. Here, using infant rats, we found that the state of AS permits the expression of theta-dependent functional connectivity between the hippocampus and RN, perhaps driving activity-dependent developmental plasticity at ages when wake-related expression of hippocampal-dependent learning has yet to emerge [69]. Importantly, given that theta oscillations in the developing hippocampal system are preferentially expressed during AS, we suggest that—under normal conditions— the state of AS promotes maximal theta-dependent coupling among structures within the hippocampal network (including the prefrontal cortex, [24]).

We did not see evidence of prominent theta during periods of wake-related movements, as occurs in the adult hippocampus [57]. Although it is possible that wake-related theta develops later, our head-fix method is incompatible with the expression of the kinds of wake behaviors (e.g., running, rearing, jumping) that accompany theta in adults. However, even in unrestrained rats, these wake behaviors are relatively infrequent at P12 [70], especially compared with AS.

Disrupted functional connectivity in neurodevelopmental disorders

Aberrant long-range connectivity occurs in such neurodevelopmental disorders as schizophrenia [71], autism [72], and ADHD [73]. Although investigations in these domains have focused largely on the cortical networks that subserve cognitive and social functions [26], it is important to acknowledge that many neurodevelopmental disorders also entail substantial sensorimotor deficits. For example, autism not only comprises cognitive and social deficits, but also deficits in motor control [74] and sensorimotor integration [75]. In addition, autism entails aberrant functional connectivity between cerebral cortex and subcortical networks involved in sensorimotor processing, including the cerebellum [76] and striatum [77]. Moreover, in children with autism, functional connectivity is specifically affected in the theta band [78].

As recently shown in the hippocampal-prefrontal system in a mouse model of schizophrenia, abnormal connectivity was detected very early in development before cognitive deficits were apparent [79]. In a similar vein, the current findings suggest that impaired functional connectivity in the rubro-hippocampal network may predict and contribute to sensorimotor

deficits; such impairments could be caused by a number of factors, including sleep disruption. Accordingly, further research into the oscillatory dynamics and state-dependent modulation of forebrain-brainstem networks has the potential to reveal common neural processes underlying the emergence of the cognitive and sensorimotor deficits of neurodevelopmental disorders.

Star Methods

Contact for reagent and resource sharing

Further information and requests for resources may be directed to, and will be fulfilled by the Lead Contact, Mark Blumberg (mark-blumberg@uiowa.edu).

Experimental models and subject details

A total of 41 male and female Sprague-Dawley Norway rats (*Rattus norvegicus*) at P7-9 (n = 11; hereafter designated as P8) and P11-13 (n = 30; hereafter designated as P12) were used. Whereas multiunit data from the RN-only recordings in the P8 and P12 subjects were published previously [12], the LFP data were newly analyzed for this study; all of the dual-recording data in the P12 subjects were collected for this study. With minor exceptions, the methods and equipment used in the two studies are identical. For all experiments, mothers and litters were housed in standard laboratory cages (48 × 20 × 26 cm). Animals were maintained on a 12:12 light-dark schedule with lights on at 0700 h and with water and food available *ad libitum*. Litters were culled to eight pups within three days of birth. Littermates were never assigned to the same experimental group. All experiments were conducted in accordance with the National Institutes of Health (NIH) Guide for the Care and Use of Laboratory Animals (NIH Publication No. 80-23) and were approved by the Institutional Animal Care and Use Committee of the University of Iowa.

Method details

Surgery—As previously described [80], a pup with a visible milk band was removed from the litter on the day of testing. Under 2-5% isoflurane anesthesia, stainless steel bipolar hook electrodes (50 μm diameter, California Fine Wire, Grover Beach, CA) were implanted into the forelimb and nuchal muscles. A ground wire was implanted transdermally on the back. After exposure and cleaning of the skull, a custom-built head-fix was attached to the skull with cyanoacrylate adhesive. The pup was allowed to recover for 1 h in a humidified incubator maintained at 35-36 °C. The pup was then briefly anesthetized again and secured in a stereotaxic apparatus (David Kopf Instruments, Tujunga, CA), where small holes were drilled in the skull for later insertion of a recording electrode into the RN (coordinates relative to bregma; P8: AP = −4.8 to -5.0 mm; ML = ±0.4 to 0.6 mm; dorsoventral (DV), 4.3 to 4.8 mm; P12: AP, −5.3 to -5.5 mm; ML, ±0.4 to 0.6 mm; DV, -5.0 to -5.5 mm) or CA1 region of hippocampus (P12: AP, −2 mm; ML, ±1.5 mm; DV, -2 to -2.5 mm; 15° lateral ang le), or a microsyringe into the medial septum (P12: AP, +1.5 mm; ML, ±1.3-1.5 mm; DV, -4.5 to 5 mm; 20° lateral angle). Two additional holes were drilled, one above the visual cortex (contralateral to the hippocampal and RN recording sites) for insertion of a ground wire (which was also used as the reference electrode), and a second in frontal cortex for insertion of a thermocouple.

General Procedure—Following surgery, pups were transferred to a stereotaxic apparatus where the animal's torso was secured to a platform; the limbs were allowed to dangle freely. To monitor brain temperature, a fine-wire thermocouple was inserted into the cerebral cortex (Omega Engineering, Stamford, CT). Brain temperature was maintained at 36-37 °C throughout all experiments. The EMG bipolar electrodes were connected to a differential amplifier (A-M Systems, Carlsborg, WA; Tucker-Davis Technologies, Alachua, FL). A stainless steel ground electrode (0.25 mm diameter; Medwire, Mt. Vernon, NY) was inserted into the cerebral cortex. Testing began after a 1-h acclimation period but not before organized sleep-wake cycles were observed.

Neurophysiological Recordings—Neural data were acquired using 16-channel silicon depth electrodes or 4-channel linear probes (NeuroNexus, Ann Arbor, MI; A1x16-Poly2-5mm-50-177; A1x16-10mm-100-177; Q1x4-10mm-50-177) connected to a data acquisition system (Cambridge Electronic Design, Cambridge, UK; Tucker-Davis Technologies). Neural and EMG signals were sampled at 25 kHz and 1 kHz, respectively. Before insertion of electrodes into the brain, the recording electrode was coated with fluorescent DiI (Vybrant DiI Cell-Labeling Solution; Life Technologies, Grand Island, NY) for subsequent histological verification of placement. During each recording session as the pup's sleep and wake behavior were manually scored by an experimenter blind to the electrophysiological record.

Pharmacological Inactivation of the Medial Septum—To assess the effects of pharmacological inactivation of the medial septum on spontaneous hippocampal and RN activity at P12, we first recorded spontaneous activity in the RN and hippocampus over a baseline period of 30 min. Then, a 0.5 μl microsyringe (Hamilton, Reno, NV) was lowered stereotaxically into the medial septum (see coordinates above). Pups received a 0.1 μl infusion into the medial septum of either fluorophore-conjugated muscimol (MUS, N = 6; ThermoFisher Scientific; 1.6 mM, dissolved in 40% dimethyl sulfoxide) or 0.9% saline (SAL, N = 6) at a rate of 0.1 μl/min. After a 15-min period to allow for drug diffusion, the 30-min post-infusion recording session began [12,81]. This infusion/recording protocol is similar to that used previously to assess the effect of inactivating the deep cerebellar nuclei (DCN; coordinates for microsyringe placement at P12: AP, -3.7 mm; ML, ±3 mm; DV, -3.2 mm; 20° lateral angle) on RN activity [12].

Histology—After testing, the pup was overdosed with ketamine/xylazine (0.08 mg/g i.p.) and perfused transcardially with phosphate-buffered saline and 4% paraformaldehyde. The brain was sliced coronally at 80 μm using a freezing microtome (Leica Microsystems, Buffalo Grove, IL). Electrode locations and drug diffusion were visualized at 2.5–5× magnification using a fluorescent microscope and digital camera (Leica Microsystems). Sections were subsequently stained with cresyl violet and electrode placements and infusion sites were confirmed.

Quantification and Statistical Analysis—All analyses and statistical tests for neural data were performed using custom-written Matlab routines (MathWorks, Natick, MA), Spike2 software (Cambridge Electronic Design), and SPSS (IBM, Armonk, NY). Alpha was

set at 0.05 for all analyses, unless otherwise stated. When repeated-measures analysis of variance (ANOVA) was performed, post hoc pairwise comparisons were performed using the Bonferroni correction procedure. Reported group data are always mean ± standard error (SE).

Behavioral State—As described previously [80], EMG signals and behavioral scoring were used to identify behavioral states. Active wake (AW) was defined as periods characterized by high-amplitude limb movements against a background of elevated muscle tone. Active sleep (AS) was defined by the presence of myoclonic twitches against a background of muscle atonia [3,82]. Twitches were identified electrographically as spikes in the EMG record with amplitudes at least 3× larger than background atonia. Behavioral quiescence (BQ) was defined as periods of low muscle tone, an absence of spiking activity in the EMG, and behaviorally confirmed absence of overt movement. Such periods typically occurred between bouts of AW and AS and were required to last at least 1 s [12].

Spike Sorting—After data acquisition, recordings were band-pass filtered (500-5000 Hz) for identification of multi-unit activity (MUA) and subsequent spike sorting. As described previously [83], spike sorting was performed using template matching and principal component analysis in Spike2. We excluded waveforms as outliers when they were larger than 3.5 SDs from the mean of a given template.

LFP Power Spectrum and Theta Ratios—For all LFP-related analyses, one LFP channel from each structure per pup was selected. Selection of the LFP channel was based on electrode placement within hippocampus or RN as well as maximum theta power during AS. Power spectra were calculated from the down-sampled LFP (1 kHz) using a 2-s Hanning window in Spike2. For time-normalization and subsequent statistical comparisons, the spectral power density values in each bin were divided by the total duration of the file comprising data for each behavioral state (see above). Theta ratios were calculated as follows: For each LFP channel and behavioral state, raw power values within theta frequency (4-7 Hz) were summed and divided by the summed raw power at 12-15 Hz; this method served to normalize values of theta power. State-dependent differences in theta ratios were calculated using repeated-measures ANOVA with theta ratio as the dependent variable. When data from two age groups were analyzed, state-dependent differences in theta ratio were calculated using a repeated-measures factorial ANOVA with age group (P8, P12) as the between-subjects factor and behavioral state (AW, BQ, AS) as the repeated-measures factor.

Twitch-Related LFP Activity—To generate individual twitch-triggered time-frequency spectrograms, the LFP signals around forelimb twitches (peri-twitch window = 1 s) were convolved using a complex Morlet wavelet. The Morlet wavelet was created as follows: the frequency band of interest (0-20 Hz) was divided into 30 bins, and the temporal resolution of the wavelet was established using a minimum of 2 and a maximum of 3 cycles. Twitch-triggered LFP theta power was calculated as follows: First, raw neural signals were filtered using a 4-7 Hz band-pass filter (IIR, Butterworth, 2^{nd} order). Next, the signal was converted using root mean square (RMS; time constant = 0.1 s). Then, data from all pups within each age or experimental group were concatenated into one file. Using forelimb twitches as

trigger events, waveform averages of theta activity were calculated in Spike2 (peri-twitch window = 2 s); we tested statistical significance by jittering twitch events 1000 times (jitter window = 1000 ms) using the interval jitter parameter settings within PatternJitter [84,85] in Matlab. We corrected for multiple comparisons using an established method [84]; this method produces upper acceptance bands to establish statistical significance for each waveform average. For analyses of twitch-related activity before and after inactivation of the medial septum (see below), we similarly created waveform averages and power spectra, both triggered on forelimb twitches and using a 2-s peri-twitch window.

LFP-LFP and Spike-LFP Coherence—LFP-LFP and Spike-LFP coherence analyses were conducted using one LFP per pup and neural structure, based on the criteria described above. Using custom-written Matlab codes, coherence analyses were calculated from cross-spectral density. Each signal was convolved using a complex Morlet wavelet. The Morlet wavelet was created as follows: the frequency band of interest (0-20 Hz) was divided into 50 bins, and the temporal resolution of the wavelet was established using a minimum of 4 and a maximum of 8 cycles. To calculate state-dependent differences in coherence, we performed repeated-measure ANOVAs for each structure with behavioral state (AW, BQ, or AS) as the repeated measure and average coherence within the theta range (4-7 Hz) as the dependent variable. Differences in spike-LFP coherence across theta conditions during AS were calculated as follows: First, we selected those spike-LFP pairs that exhibited a coherence peak within the theta frequency range (4-7 Hz) for periods of high-amplitude theta (see below). Then, we calculated statistical differences across theta amplitude conditions using repeated-measures ANOVAs, with coherence values within the theta-frequency range as the dependent variable.

Granger Causality—Wiener-Granger causality analyses were conducted using the same LFPs per pup and neural structure selected above. The linear regression model used in this analysis aimed to calculate, for two structures, the prediction error for a current LFP data point in one structure based on past LFP data points in the other structure. Hipp→RN and RN→Hipp prediction errors were calculated using a function adapted from the BSMART toolbox [35,86]. The LFP data across the entire session for each pup were divided into sequential 2-s segments to provide a sufficient number of samples for Granger analysis. Statistical significance for Granger causality was assessed against a null-hypothesis baseline distribution [24,87] generated using a bootstrap-shuffle (n = 100 shuffles) in which the 2-s segments of hippocampal and RN LFP data were randomly paired. The same calculation was conducted with 3-s temporal segments to confirm that the obtained results were not sensitive to the chosen segment size. For those pups that exhibited significant Granger values (hippocampus→RN or RN→hippocampus) during AS, we performed related-samples t tests using peak Granger value as the dependent variable to assess differences in strength between the two directions.

LFP Cross-Correlation—The amount of temporal synchrony between hippocampal and RN theta oscillations (4-7 Hz) was measured by cross-correlating the two band-pass-filtered LFP signals (bin resolution = 1 ms). Cross-correlation analyses were conducted using the same LFPs per pup and neural structure selected above. The hippocampal signal was always

the driving signal. For this analysis, entire bouts of AS were divided into 2-s segments to compute average theta power.

The correlation coefficient in each calculation was compared with the value produced using a bootstrap-shuffle method (n = 1000) applied to the hippocampal LFP; for this method, in each iteration we selected a random point on the LFP and switched the 2-s segments on either side of that point. To verify that the current results were not obtained by chance, the same calculations were performed using different segment sizes (1-s and 5-s segments); the results with different temporal segments were not quantitatively or qualitatively different. Differences between original and shuffled data were calculated using independent-samples t tests with the cross-correlation coefficient as the dependent variable.

Phase Locking—Theta phases were calculated by applying the Hilbert transform to the band-pass-filtered theta rhythms in the hippocampus or RN [88]. Rayleigh's tests were used to determine whether MUA signals were significantly phase-locked to the theta (4-7 Hz) oscillation [69,89]. For this test, a phase estimate was first assigned to each spike time and a phase histogram (20 degree/bin) was generated for each MUA signal. Next, the phase-locking value (PLV) was calculated to quantify the amount of phase-locking [90,91]. Z-transformed PLVs were calculated by using a bootstrap-shuffle method (n = 1000); for this method, in each iteration we selected a random point on the LFP and switched the segments on either side of that point. If both Rayleigh's test and the Z-transformed PLV were statistically significant for a given MUA signal, the MUA signal was regarded as significantly phase-locked to the theta rhythm for that structure. We calculated statistical differences across theta amplitude conditions using repeated-measures ANOVA, with PLVs within the theta-frequency range as the dependent variable.

Inactivation of the Medial Septum—To assess the effect of medial septum inactivation on sleep measures, we calculated mean time spent in AS and mean twitching rates during the pre- and post-infusion recording periods. Twitching rates were calculated by dividing the total number of twitches in each muscle group (forelimb, nuchal) by total time spent in AS. To assess statistical differences in these sleep measures, we performed independent pairwise comparisons (pre- vs. post-inactivation) using the Wilcoxon matched-pairs signed-ranks tests. Effects of medial septum inactivation on theta activity during AS were statistically evaluated using a 2 × 2 repeated-measures factorial ANOVA with experimental group (MUS or SAL) as the between-subjects factor and time (Pre or Post) as the repeated-measures factor. For this analysis, theta ratios in each structure (see above) were used as the dependent variables. The same analytical approach was adopted to evaluate the effects of inactivation of the deep cerebellar nuclei (DCN) on oscillatory activity in the RN; this last analysis was performed using data from a previously published study [12].

Supplementary Material

Refer to Web version on PubMed Central for supplementary material.

Acknowledgments

We thank Brian Bland, György Buzsáki, Alex Tiriac, and Jimmy Dooley for helpful suggestions. This research was supported by National Institute of Child Health and Human Development Grant R37-HD081168 to M. S. Blumberg. C. Del Rio-Bermudez was supported by the Fulbright Foreign Student Program.

References

1. Roffwarg HP, Muzio JN, Dement WC. Ontogenetic development of the human sleep-dream cycle. Science. 1966; 152:604–619. [PubMed: 17779492]
2. Jouvet-Mounier D, Astic L, Lacote D. Ontogenesis of the states of sleep in rat, cat, and guinea pig during the first postnatal month. Dev Psychobiol. 1970; 2:216–239. [PubMed: 5527153]
3. Blumberg, MS., Seelke, AMH. The form and function of infant sleep: From muscle to neocortex. In: Blumberg, MS.Freeman, JH., Robinson, SR., editors. The Oxford Handbook of Developmental Behavioral Neuroscience. New York: Oxford University Press; 2010. p. 391-423.
4. Kayser MS, Biron D. Sleep and development in genetically tractable model organisms. Genetics. 2016; 203:21–33. [PubMed: 27183564]
5. Frank MG. Sleep and developmental plasticity: Not just for kids. Prog Brain Res. 2011; 193:221–232. [PubMed: 21854965]
6. Blumberg MS, Marques HG, Iida F. Twitching in sensorimotor development from sleeping rats to robots. Curr Biol. 2013; 23:R532–R537. [PubMed: 23787051]
7. Khazipov R, Sirota A, Leinekugel X, Holmes GL, Ben-Ari Y, Buzsáki G. Early motor activity drives spindle bursts in the developing somatosensory cortex. Nature. 2004; 432:758–61. [PubMed: 15592414]
8. Petersson P, Waldenström A, Fåhraeus C, Schouenborg J. Spontaneous muscle twitches during sleep guide spinal self-organization. Nature. 2003; 424:72–75. [PubMed: 12840761]
9. Tiriac A, Sokoloff G, Blumberg MS. Myoclonic twitching and sleep-dependent plasticity in the developing sensorimotor system. Curr Sleep Med Reports. 2015; 1:74–79.
10. Del Rio-Bermudez C, Sokoloff G, Blumberg MS. Sensorimotor processing in the newborn rat red nucleus during active sleep. J Neurosci. 2015; 35:8322–32. [PubMed: 26019345]
11. Flumerfelt BA. An ultrastructural investigation of afferent connections of the red nucleus in the rat. J Anat. 1980; 131:621–633. [PubMed: 7216902]
12. Del Rio-Bermudez C, Plumeau AM, Sattler NJ, Sokoloff G, Blumberg MS. Spontaneous activity and functional connectivity in the developing cerebellorubral system. J Neurophysiol. 2016; 116:1316–1327. [PubMed: 27385801]
13. Giuffrida R, Volsi GL, Perciavalle V. Influences of cerebral cortex and cerebellum on the red nucleus of the rat. Behav Brain Res. 1988; 28:109–111. [PubMed: 2838036]
14. Dypvik AT, Bland BH. Functional connectivity between the red nucleus and the hippocampus supports the role of hippocampal formation in sensorimotor integration. J Neurophysiol. 2004; 92:2040–2050. [PubMed: 15175366]
15. Nioche C, Cabanis EA, Habas C. Functional connectivity of the human red nucleus in the brain resting state at 3T. Am J Neuroradiol. 2009; 30:396–403. [PubMed: 19022864]
16. Ryou JW, Cho SY, Kim HT. Lesion of the cerebellar interpositus nucleus or the red nucleus affects classically conditioned neuronal activity in the hippocampus. Prog Neuro-Psychopharmacology Biol Psychiatry. 1998; 22:169–185.
17. Bird CM, Burgess N. The hippocampus and memory: insights from spatial processing. Nat Rev Neurosci. 2008; 9:182–194. [PubMed: 18270514]
18. Bast T. Toward an integrative perspective on hippocampal function: from the rapid encoding of experience to adaptive behavior. Rev Neurosci. 2007; 18:253–281. [PubMed: 18019609]
19. Vanderwolf CH. The hippocampus as an olfacto-motor mechanism: were the classical anatomists right after all? Behav Brain Res. 2001; 127:25–47. [PubMed: 11718883]
20. Bland BH, Oddie SD. Theta band oscillation and synchrony in the hippocampal formation and associated structures: the case for its role in sensorimotor integration. Behav Brain Res. 2001; 127:119–136. [PubMed: 11718888]

21. Buzsáki G, Draguhn A. Neuronal oscillations in cortical networks. Science. 2004; 304:1926–9. [PubMed: 15218136]
22. Fujisawa S, Buzsáki G. A 4 Hz Oscillation adaptively synchronizes prefrontal, VTA, and hippocampal activities. Neuron. 2011; 72:153–165. [PubMed: 21982376]
23. Karalis N, Dejean C, Chaudun F, Khoder S, Rozeske RR, Wurtz H, Bagur S, Benchenane K, Sirota A, Courtin J, et al. 4-Hz oscillations synchronize prefrontal-amygdala circuits during fear behavior. Nat Neurosci. 2016; 19:605–12. [PubMed: 26878674]
24. Brockmann MD, Poschel B, Cichon N, Hanganu-Opatz IL. Coupled oscillations mediate directed interactions between prefrontal cortex and hippocampus of the neonatal rat. Neuron. 2011; 71:332–347. [PubMed: 21791291]
25. Hanganu-Opatz IL. Between molecules and experience: role of early patterns of coordinated activity for the development of cortical maps and sensory abilities. Brain Res Rev. 2010; 64:160–176. [PubMed: 20381527]
26. Uhlhaas PJ, Roux F, Rodriguez E, Rotarska-Jagiela A, Singer W. Neural synchrony and the development of cortical networks. Trends Cogn Sci. 2010; 14:72–80. [PubMed: 20080054]
27. Khazipov R, Luhmann HJ. Early patterns of electrical activity in the developing cerebral cortex of humans and rodents. Trends Neurosci. 2006; 29:414–418. [PubMed: 16713634]
28. Ekstrom AD, Caplan JB, Ho E, Shattuck K, Fried I, Kahana MJ. Human hippocampal theta activity during virtual navigation. Hippocampus. 2005; 15:881–889. [PubMed: 16114040]
29. Grion N, Akrami A, Zuo Y, Stella F, Diamond ME. Coherence between rat sensorimotor system and hippocampus is enhanced during tactile discrimination. PLoS Biol. 2016; 14
30. Mohns EJ, Blumberg MS. Synchronous bursts of neuronal activity in the developing hippocampus: modulation by active sleep and association with emerging gamma and theta rhythms. J Neurosci. 2008; 28:10134–10144. [PubMed: 18829971]
31. Tiriac A, Del Rio-Bermudez C, Blumberg MS. Self-generated movements with “unexpected” sensory consequences. Curr Biol. 2014; 24:2136–2141. [PubMed: 25131675]
32. Montgomery SM, Sirota A, Buzsáki G. Theta and gamma coordination of hippocampal networks during waking and rapid eye movement sleep. J Neurosci. 2008; 28:6731–6741. [PubMed: 18579747]
33. Wills TJ, Cacucci F, Burgess N, O'Keefe J. Development of the hippocampal cognitive map in preweanling rats. Science. 2010; 328:1573–1576. [PubMed: 20558720]
34. Granger CWJ. Investigating Causal Relations by Econometric Models and Cross-spectral Methods. Econometrica. 1969; 37:424–438.
35. Cui J, Xu L, Bressler SL, Ding M, Liang H. BSMART: A Matlab/C toolbox for analysis of multichannel neural time series. Neural Networks. 2008; 21:1094–1104. [PubMed: 18599267]
36. De Zeeuw CI, Hoogenraad CC, Koekkoek SKE, Ruigrok TJH, Galjart N, Simpson JI. Microcircuitry and function of the inferior olive. Trends Neurosci. 1998; 21:391–400. [PubMed: 9735947]
37. Vertes RP, Kocsis B. Brainstem-diencephalo-septohippocampal systems controlling the theta rhythm of the hippocampus. Neuroscience. 1997; 81:893–926. [PubMed: 9330355]
38. Allen CN, Crawford IL. GABAergic agents on the medial septal nucleus affect hippocampal theta rhythm and acetylcholine utilization. Brain Res. 1984; 322:261–267. [PubMed: 6509317]
39. Naus C, Flumerfelt BA, Hrycyshyn AW. An anterograde HRP-WGA study of aberrant corticorubral projections following neonatal lesions of the rat sensorimotor cortex. Exp Brain Res. 1985; 59:365–371. [PubMed: 2411584]
40. Mohns EJ, Blumberg MS. Neocortical activation of the hippocampus during sleep in infant rats. J Neurosci. 2010; 30:3438–3449. [PubMed: 20203203]
41. Williams, PTJa, Kim, S., Martin, JH. Postnatal maturation of the red nucleus motor map depends on rubrospinal connections with forelimb motor pools. J Neurosci. 2014; 34:4432–41. [PubMed: 24647962]
42. Torres F, Anderson C. The normal EEG of the human newborn. J Clin Neurophysiol. 1985; 2:89–103. [PubMed: 3916842]

43. Vanhatalo S, Kaila K. Development of neonatal EEG activity: From phenomenology to physiology. Semin Fetal Neonatal Med. 2006; 11:471–478. [PubMed: 17018268]
44. Sokoloff G, Plumeau AM, Mukherjee D, Blumberg MS. Twitch-related and rhythmic activation of the developing cerebellar cortex. J Neurophysiol. 2015; 114:1746–1756. [PubMed: 26156383]
45. Danglot L, Triller A, Marty S. The development of hippocampal interneurons in rodents. Hippocampus. 2006; 16:1032–1060. [PubMed: 17094147]
46. Bender R, Plaschke M, Naumann T, Wahle P, Frotscher M. Development of cholinergic and GABAergic neurons in the rat medial septum: different onset of choline acetyltransferase and glutamate decarboxylase mRNA expression. J Comp Neurol. 1996; 372:204–214. [PubMed: 8863126]
47. de Lecea L, del Río Ja, Soriano E. Developmental expression of parvalbumin mRNA in the cerebral cortex and hippocampus of the rat. Brain Res Mol Brain Res. 1995; 32:1–13. [PubMed: 7494447]
48. Buzsáki G, Lai-Wo SL, Vanderwolf CH. Cellular bases of hippocampal EEG in the behaving rat. Brain Res Rev. 1983; 6:139–171.
49. Amilhon B, Huh CYL, Dé F, Manseau R, Ducharme G, Nichol H, Adamantidis A, Williams S. Parvalbumin interneurons of hippocampus tune population activity at theta frequency. Neuron. 2015; 86:1277–1289. [PubMed: 26050044]
50. Ciranna L, Licata F, Li Volsi G, Santangelo F. Neurotransmitter-mediated control of neuronal firing in the red nucleus of the rat: reciprocal modulation between noradrenaline and GABA. Exp Neurol. 2000; 163:253–63. [PubMed: 10785465]
51. Hontanilla B, Parent A, Giménez-Amaya JM. Heterogeneous distribution of neurons containing calbindin D-28k and/or parvalbumin in the rat red nucleus. Brain Res. 1995; 696:121–126. [PubMed: 8574659]
52. Fu YS, Tseng GF, Ying HS. The postnatal development of the gaba a/benzodiazepine receptor in the rat red nucleus. J Recept Res. 1994; 14:267–280. [PubMed: 8083869]
53. Bernays RL, Heeb L, Cuenod M, Streit P. Afferents to the rat red nucleus studied by means of d-[3H] aspart ate, [3H]choline and non-selective tracers. Neuroscience. 1988; 26:601–619. [PubMed: 3173690]
54. Ricardo JA. Efferent connections of the subthalamic region in the rat. II. The zona incerta. Brain Res. 1981; 214:43–60. [PubMed: 7237165]
55. Staiger JF, Wouterlood FG. Efferent projections from the lateral septal nucleus to the anterior hypothalamus in the rat: A study combining Phaseolus vulgaris-leucoagglutinin tracing with vasopressin immunocytochemistry. Cell Tissue Res. 1990; 261:17–23. [PubMed: 2383883]
56. Buzsáki, G. Rhythms of the Brain. New York: Oxford University Press; 2006.
57. Bland BH. The physiology and pharmacology of hippocampal formation theta rhythms. Prog Neurobiol. 1986; 26:1–54. [PubMed: 2870537]
58. Robinson TE, Kramis RC, Vanderwolf CH. Two types of cerebral activation during active sleep: relations to behavior. Brain Res. 1977; 124:544–549. [PubMed: 192415]
59. Bland SK, Bland BH. Medial septal modulation of hippocampal theta cell discharges. Brain Res. 1986; 375:102–116. [PubMed: 3719349]
60. Tiriac A, Blumberg MS. The case of the disappearing spindle burst. Neural Plast. 2016; 2016
61. Rathelot JA, Padel Y. Ascending spinal influences on rubrospinal cells in the cat. Exp Brain Res. 1997; 116:326–340. [PubMed: 9348131]
62. Christian KM, Thompson RF. Neural substrates of eyeblink conditioning: acquisition and retention. Learn Mem (Cold Spring Harb NY). 2003; 10:427–455.
63. Hoffmann LC, Berry SD. Cerebellar theta oscillations are synchronized during hippocampal theta-contingent trace conditioning. Proc Natl Acad Sci U S A. 2009; 106:21371–6. [PubMed: 19940240]
64. Bender F, Gorbati M, Cadavieco MC, Denisova N, Gao X, Holman C, Korotkova T, Ponomarenko A. Theta oscillations regulate the speed of locomotion via a hippocampus to lateral septum pathway. Nat Commun. 2015; 6:8521. [PubMed: 26455912]

65. Morris R, Vallester KK, Newton SS, Kearsley AP, Whishaw IQ. The differential contributions of the parvocellular and the magnocellular subdivisions of the red nucleus to skilled reaching in the rat. Neuroscience. 2015; 295:48–57. [PubMed: 25813707]
66. Power JD, Fair DA, Schlaggar BL, Petersen SE. The Development of Human Functional Brain Networks. Neuron. 2010; 67:735–748. [PubMed: 20826306]
67. Popa D, Duvarci S, Popescu AT, Léna C, Paré D. Coherent amygdalocortical theta promotes fear memory consolidation during paradoxical sleep. Proc Natl Acad Sci U S A. 2010; 107:6516–9. [PubMed: 20332204]
68. Boyce R, Glasgow SD, Williams S, Adamantidis AR. Causal evidence for the role of REM sleep theta rhythm in contextual memory consolidation. Science. 2016; 352:812–816. [PubMed: 27174984]
69. Kim J, Goldsberry ME, Harmon TC, Freeman JH. Developmental changes in hippocampal ca1 single neuron firing and theta activity during associative learning. PLoS One. 2016; 11:e0164781. [PubMed: 27764172]
70. Altman J, Sudarshan K. Postnatal development of locomotion in the laboratory rat. Anim Behav. 1975; 23:896–920. [PubMed: 1200422]
71. Whitfield-Gabrieli AS, Thermenos HW, Milanovic S, Tsuang MT, Faraone SV, Mccarley RW, Shenton ME, Green AI, Nieto-Castanon A, Laviolette P, et al. Hyperactivity and hyperconnectivity of the default Hyperactivity in schizophrenia and in first-degree network relatives with schizophrenia of persons. Proc Natl Acad Sci U S A. 2013; 106:1279–1284.
72. Kennedy DP, Redcay E, Courchesne E. Failing to deactivate: resting functional abnormalities in autism. Proc Natl Acad Sci U S A. 2006; 103:8275–8280. [PubMed: 16702548]
73. Uddin LQ, Kelly AMC, Biswal BB, Margulies DS, Shehzad Z, Shaw D, Ghaffari M, Rotrosen J, Adler LA, Castellanos FX, et al. Network homogeneity reveals decreased integrity of default-mode network in ADHD. J Neurosci Methods. 2008; 169:249–254. [PubMed: 18190970]
74. Vanvuchelen M, Roeyers H, De Weerdt W. Nature of motor imitation problems in school-aged boys with autism: a motor or a cognitive problem? Autism. 2007; 11:225–240. [PubMed: 17478576]
75. Hannant P, Cassidy S, Tavassoli T, Mann F. Sensorimotor difficulties are associated with the severity of autism spectrum conditions. Front Integr Neurosci. 2016; 10:1–14. [PubMed: 26834584]
76. Wang SSH, Kloth AD, Badura A. The Cerebellum, Sensitive Periods, and Autism. Neuron. 2014; 83:518–532. [PubMed: 25102558]
77. Takarae Y, Minshew NJ, Luna B, Sweeney JA. Atypical involvement of frontostriatal systems during sensorimotor control in autism. Psychiatry Res - Neuroimaging. 2007; 156:117–127. [PubMed: 17913474]
78. Kikuchi M, Yoshimura Y, Hiraishi H, Munesue T, Hashimoto T, Tsubokawa T, Takahashi T, Suzuki M, Higashida H, Minabe Y. Reduced long-range functional connectivity in young children with autism spectrum disorder. Soc Cogn Affect Neurosci. 2015; 10:248–254. [PubMed: 24652855]
79. Hartung H, Cichon N, De Feo V, Riemann S, Schildt S, Lindemann C, Mulert C, Gogos JA, Hanganu-Opatz IL. From Shortage to Surge: A Developmental Switch in Hippocampal-Prefrontal Coupling in a Gene-Environment Model of Neuropsychiatric Disorders. Cereb Cortex. 2016:4265–4281. [PubMed: 27613435]
80. Blumberg MS, Sokoloff G, Tiriac A, Del Rio-Bermudez C. A valuable and promising method for recording brain activity in behaving newborn rodents. Dev Psychobiol. 2015; 57:506–517. [PubMed: 25864710]
81. Allen TA, Narayanan NS, Kholodar-Smith DB, Zhao Y, Laubach M, Brown TH. Imaging the spread of reversible brain inactivations using fluorescent muscimol. J Neurosci Methods. 2008; 171:30–38. [PubMed: 18377997]
82. Seelke AMH, Blumberg MS. The microstructure of active and quiet sleep as cortical delta activity emerges in infant rats. Sleep. 2008; 31:691–9. [PubMed: 18517038]
83. Sokoloff G, Uitermarkt BD, Blumberg MS. REM sleep twitches rouse nascent cerebellar circuits: Implications for sensorimotor development. Dev Neurobiol. 2015; 75:1140–1153. [PubMed: 24677804]

84. Amarasingham A, Harrison MT, Hatsopoulos NG, Geman S. Conditional modeling and the jitter method of spike re-sampling. J Neurophysiol. 2012; 107:517–531. [PubMed: 22031767]

85. Harrison MT, Geman S. A rate and history-preserving resampling algorithm for neural spike trains. Neural Comuptation. 2009; 21:1244–1258.

86. Cohen XM. Analyzing Neural Time Series Data. 2014

87. Brovelli A, Ding M, Ledberg A, Chen Y, Nakamura R, Bressler SL. Beta oscillations in a large-scale sensorimotor cortical network: directional influences revealed by Granger causality. Proc Natl Acad Sci U S A. 2004; 101:9849–54. [PubMed: 15210971]

88. Le Van Quyen M, Foucher J, Lachaux J, Rodriguez E, Lutz a, Martinerie J, Varela FJ. Comparison of Hilbert transform and wavelet methods for the analysis of neuronal synchrony. J Neurosci Methods. 2001; 111:83–98. [PubMed: 11595276]

89. Kim J, Delcasso S, Lee I. Neural Correlates of Object-in-Place Learning in Hippocampus and Prefrontal Cortex. J Neurosci. 2011; 31:16991–17006. [PubMed: 22114269]

90. Nokia MS, Penttonen M, Korhonen T, Wikgren J. Hippocampal theta (3-8Hz) activity during classical eyeblink conditioning in rabbits. Neurobiol Learn Mem. 2008; 90:62–70. [PubMed: 18294872]

91. Wikgren J, Nokia MS, Penttonen M. Hippocampo-cerebellar theta band phase synchrony in rabbits. Neuroscience. 2010; 165:1538–1545. [PubMed: 19945512]

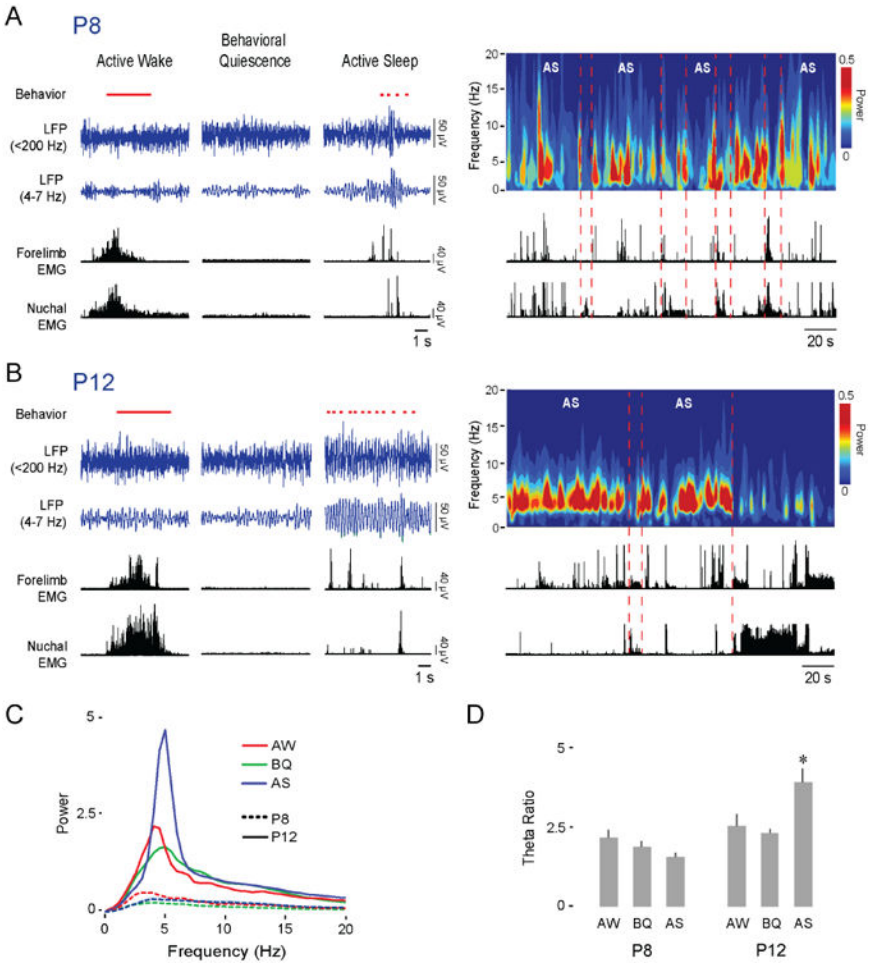

Figure 1. The infant RN exhibits AS-dependent theta oscillations

(A) Left: Representative data in a P8 rat depicting sleep and wake behavior (wake movements: horizontal red line; twitches: red ticks; manually scored), RN LFP (blue traces), and forelimb and nuchal EMGs (black traces) across behavioral states. Right: Representative time-frequency spectrogram and associated EMG activity at P8 as pup cycles in and out of AS.

(B) Same as in (A) but at P12.

(C) Mean power spectra of LFP activity in the RN of P8 (11 pups, dashed lines) and P12 (n = 11 pups, continuous lines) rats during AW (red), BQ (green), and AS (blue).

(D) Mean (+ SE) theta ratio for P8 and P12 rats during AW, BQ, and AS. Asterisk indicates significant difference from other behavioral states at P12, $p < 0.002$.

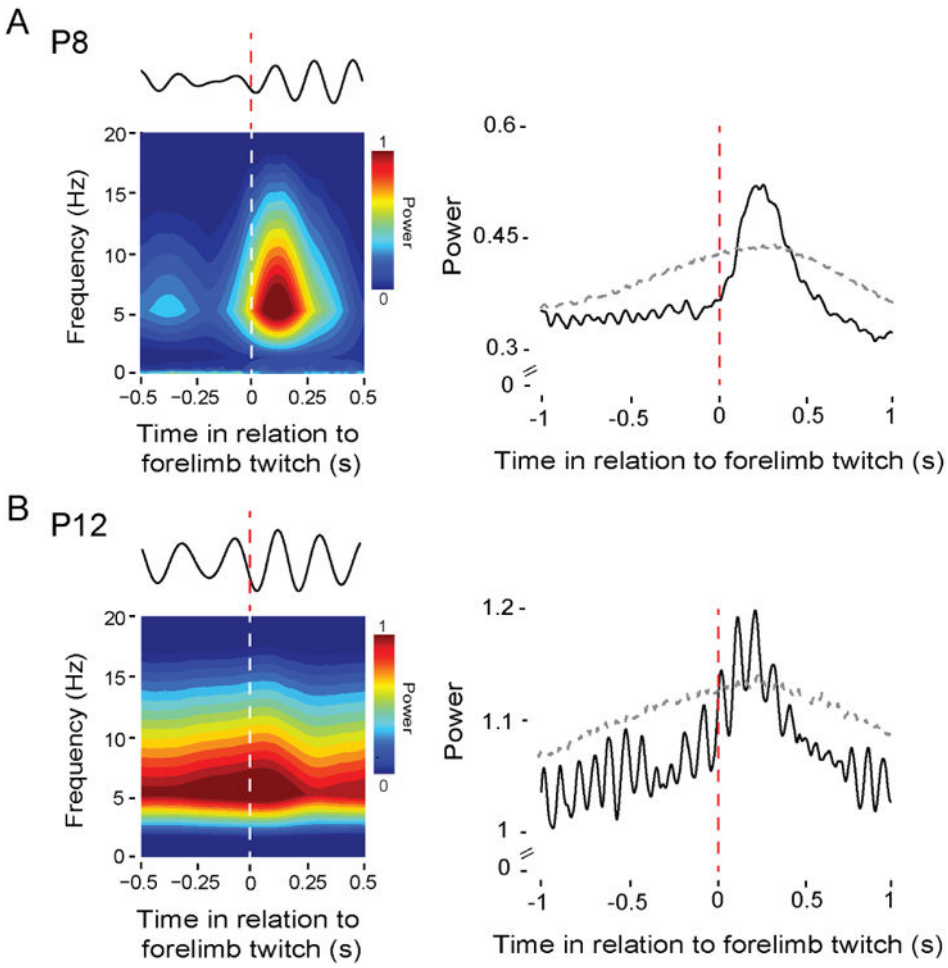

Figure 2. Myoclonic twitches trigger theta oscillations in the RN

(A) Left: Twitch-triggered time-frequency spectrogram for a representative P8 rat (108 forelimb twitches). Above the spectrogram is a representative LFP signal (4-7 Hz) from the same pup in response to a single forelimb twitch. Right: Mean twitch-triggered LFP power (4-7 Hz, root mean square) pooled across subjects (11 pups; 2,292 forelimb twitches). Horizontal dashed line denotes upper acceptance band, $p < 0.01$.

(B) Left: Same as in (A) but at P12 (147 forelimb twitches). Right: Same as in (A) but at P12 (11 pups; 1,054 forelimb twitches).

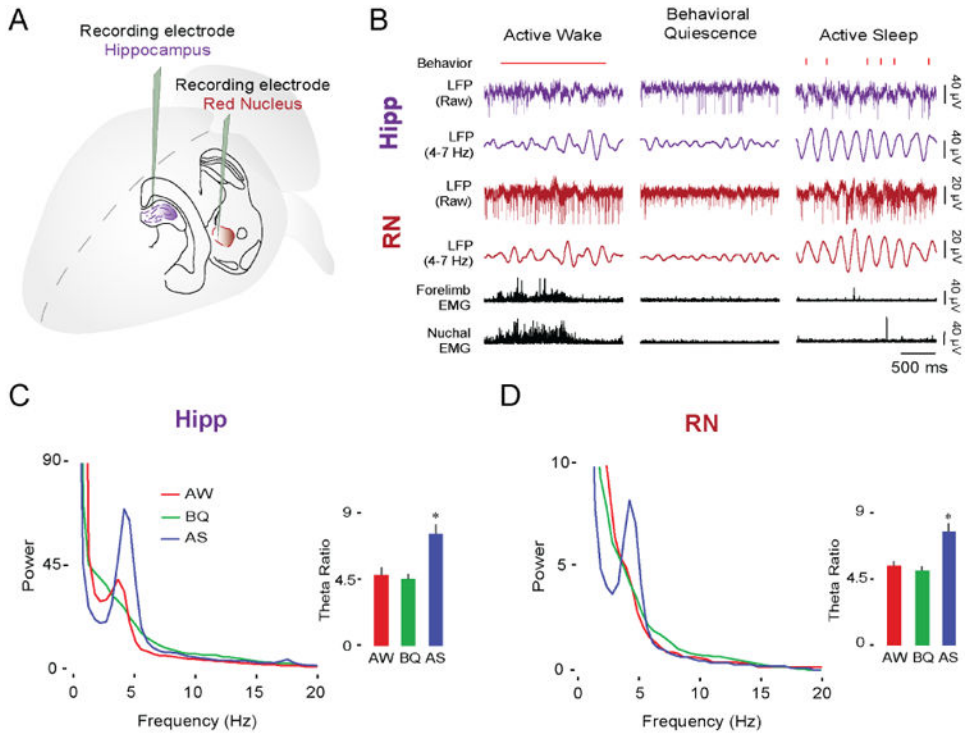

Figure 3. The hippocampus and RN exhibit similar state-dependent theta activity at P12

(A) Illustration depicting electrode placements in the dorsal hippocampus and RN.

(B) Representative data from a P12 rat showing sleep and wake behavior (wake movements: horizontal red line; twitches: red ticks; manually scored), simultaneously recorded LFP activity in the hippocampus (purple traces) and RN (red traces), and forelimb and nuchal EMGs (black traces) across behavioral states.

(C) Mean LFP power spectra and mean (+ SE) theta ratios in the hippocampus at P12 (19 pups) during AW (red), BQ (green), and AS (blue). Asterisk denotes significant difference from other behavioral states, $p < 0.001$.

(D) Same as in (C) but for RN.

See also Figure S2 and Figure S4.

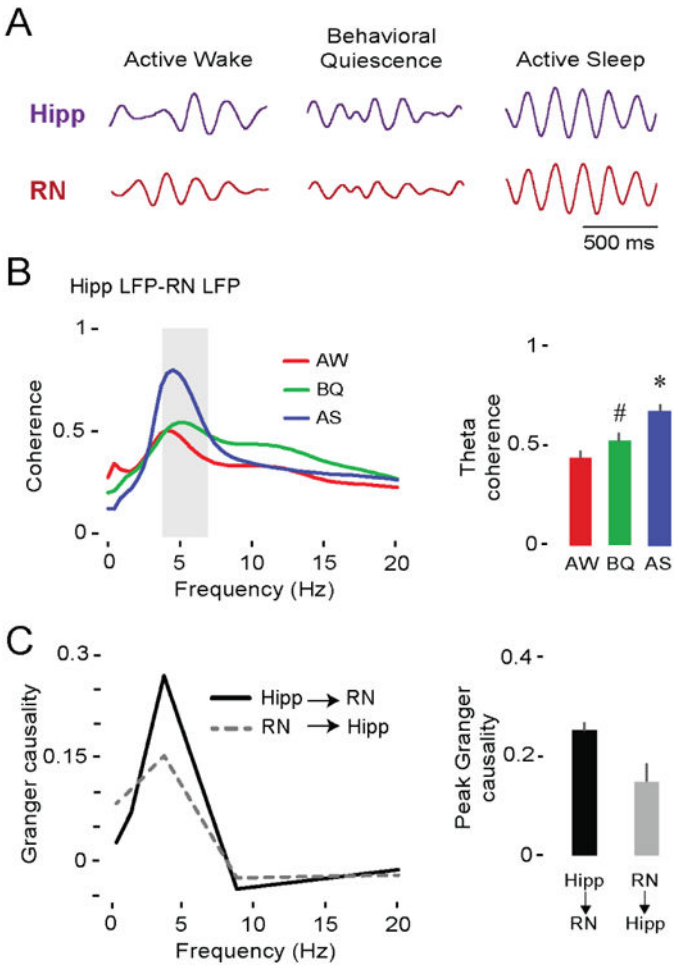

Figure 4. Theta oscillations in the hippocampus and RN at P12 are coherent and mutually interactive during AS

(A) Representative theta-filtered LFPs (4-7 Hz) in the hippocampus (purple trace) and RN (red trace) in a P12 rat across behavioral states.

(B) Left: Mean LFP-LFP coherence spectra between hippocampus and RN (19 pups, 19 LFP pairs) during AW (red), BQ (green), and AS (blue). Shaded gray area indicates theta-frequency range. Right: Mean (+ SE) theta coherence across behavioral states. Asterisk denotes significant difference from AW and BQ, $p < 0.001$. Hashtag indicates significant difference from AW, $p < 0.05$.

(C) Left: Mean Granger causality spectra for pups exhibiting significant bidirectional interactions between hippocampus and RN ($p < 0.01$; 9 pups, 9 LFP pairs). Right: Mean (+ SE) peak Granger causality value within theta-frequency range (9 pups, 9 LFP pairs). See also Figure S4.

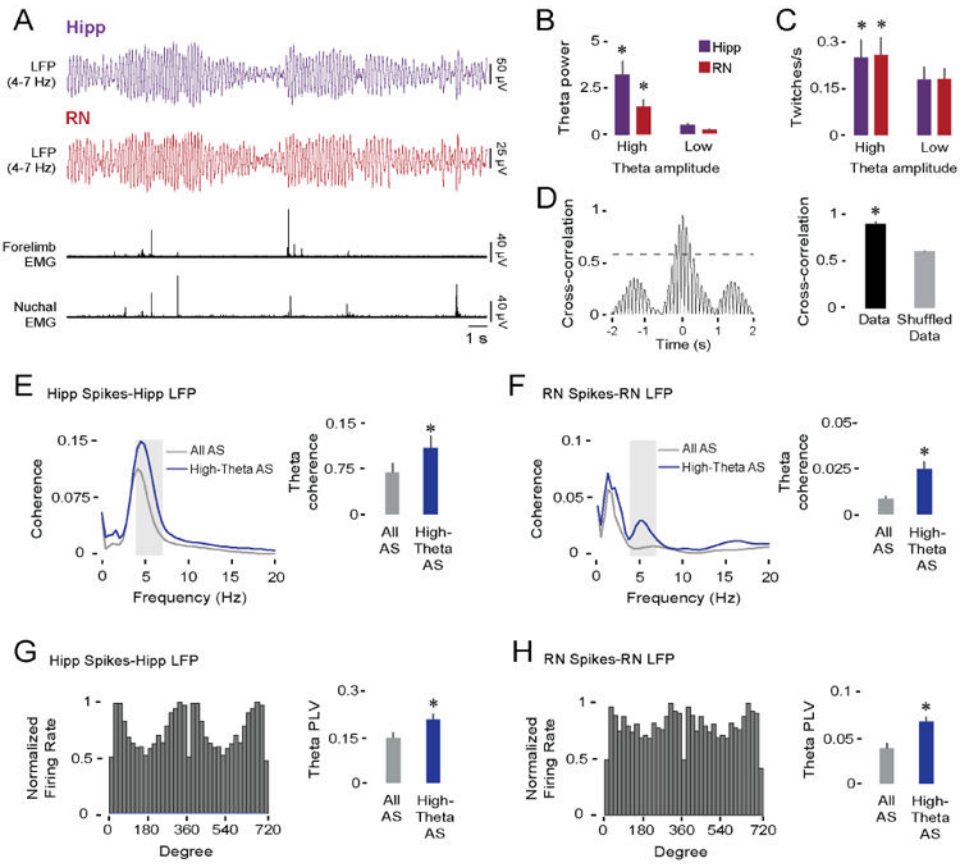

Figure 5. Comodulation of theta in the hippocampus and RN during AS at P12

(A) Representative data in a P12 rat depicting simultaneously recorded theta-filtered LFPs (4-7 Hz) in the hippocampus (purple trace) and RN (red trace), and forelimb and nuchal EMGs (black traces).

(B) Mean (+ SE) theta power in the hippocampus (purple bars) and RN (red bars) during periods of high- and low-amplitude theta (19 pups). Asterisks denote significant difference from low-amplitude theta values, $p < 0.001$.

(C) Same as in (B) but for twitching rate.

(D) Left: Representative cross-correlogram between theta-filtered LFPs in the hippocampus and RN of a P12 rat. Dashed line denotes threshold for statistical significance, $p < .01$. Right: Mean (+ SE) LFP cross-correlation coefficients between hippocampus and RN for actual and shuffled data (19 pups, 19 LFP pairs). Asterisk denotes significant difference, $p < 0.001$.

(E) Left: Averaged hippocampal spike-LFP coherence spectra during entire periods of AS (gray line) and periods of AS with high-amplitude theta (blue line; 27 spike-LFP pairs). Shaded gray area indicates theta-frequency range. Right: Mean (+ SE) spike-LFP coherence within the theta-frequency range. Asterisk denotes significant difference, $p < 0.004$.

(F) Same as in (E) but for RN spike-LFP coherence (27 spike-LFP pairs).

(G) Left: Representative example of significant phase-locked spiking activity in the hippocampus. Right: Mean phase-locking values within the theta-frequency range during

entire periods of AS (gray bar) and periods of AS with high-amplitude theta (blue bar; 27 spike-LFP pairs). Asterisk denotes significant difference, $p < 0.005$.
(H) Same as in (G) but for RN phase-locking (36 spike-LFP pairs).
See also Figure S1 and Figure S4.

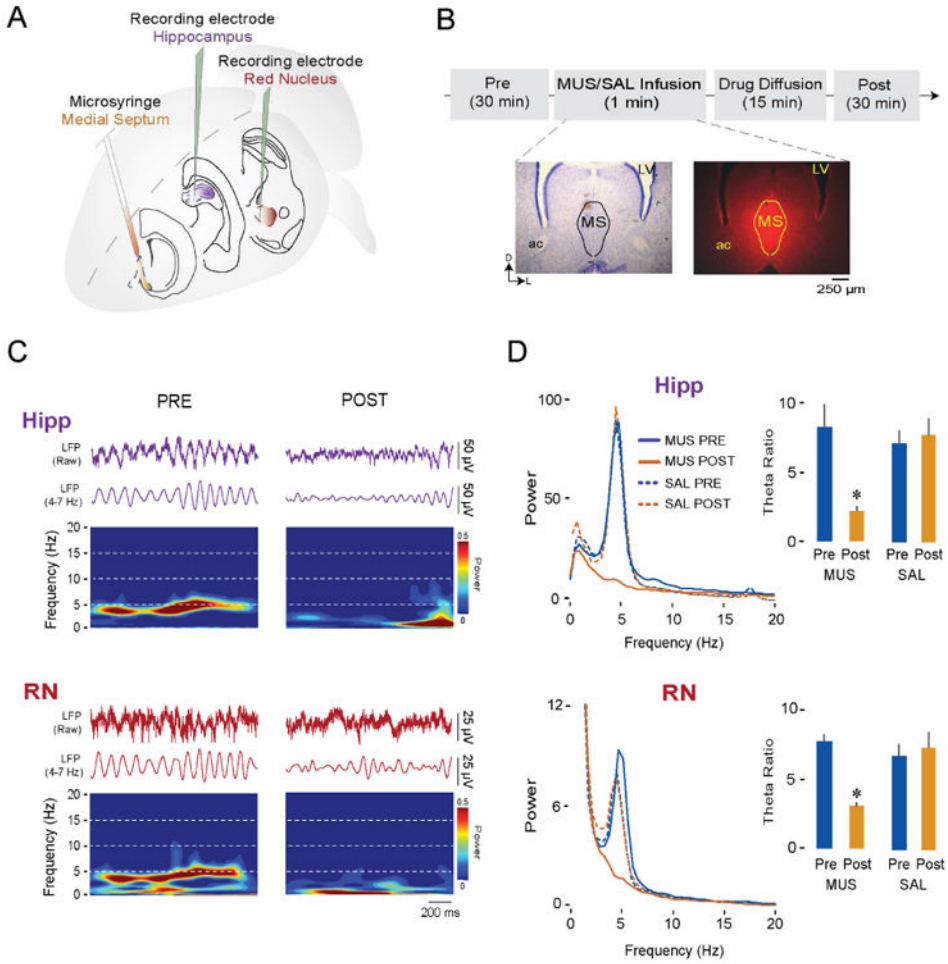

Figure 6. Pharmacological inactivation of the medial septum (MS) blocks theta oscillations in both the hippocampus and RN at P12

(A) Illustration depicting electrode placements in the hippocampus and RN and microsyringe placement in the MS.

(B) Experimental timeline and representative coronal Nissl-stained brain section (left) and corresponding section showing diffusion of fluorescent muscimol in the MS (right). LV = lateral ventricle; ac = anterior commissure.

(C) Representative dual LFP recordings during AS in a P12 rat from the hippocampus (purple traces) and RN (red traces) and corresponding time-frequency spectrograms. (D) Left: Averaged LFP power spectra during AS in the hippocampus (top) and RN (bottom) before (Pre) and after (Post) infusion of either muscimol (MUS; 6 pups) or saline (SAL; 6 pups) into the MS. Right: Mean (+ SE) theta ratios during AS in the hippocampus (top) and RN (bottom) before and after infusion of muscimol or saline into the MS. Asterisks indicate significant difference from Pre, $p < 0.02$.

See also Figure S3, Figure S4, and Table S1.

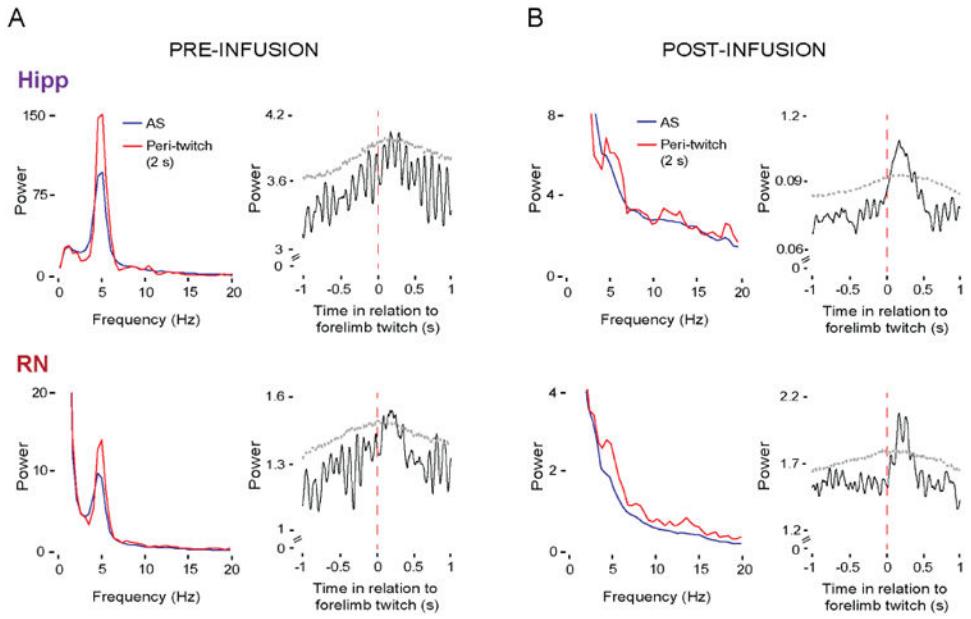

Figure 7. Twitch-triggered theta oscillations are preserved in the hippocampus and RN after pharmacological inactivation of the medial septum (MS) at P12

(A) Left: Averaged LFP power spectra in the hippocampus (top) and RN (bottom) across periods of AS (blue lines) and periods around twitches (red lines) across P12 subjects (6 pups) before infusion of muscimol into the MS. Right: Mean twitch-triggered LFP power (4-7 Hz, root mean square) for the hippocampus (top) and RN (bottom) pooled across subjects (6 pups; 256 forelimb twitches). Horizontal dashed lines denote upper acceptance bands, $p < 0.05$.

(B) Same as in (A) but after infusion of muscimol into the MS. Data for mean twitch-triggered LFP power are from 305 forelimb twitches pooled across six pups.

See also Figure S4.

Table 1

Key Resources Table

REAGENT or RESOURCE	SOURCE	IDENTIFIER
Chemicals, Peptides, and Recombinant Proteins		
Vybrant DiI Cell-Labeling Solution	Life Technologies	Cat #: V22885
Muscimol, BODIPY ® TMR-X Conjugate	ThermoFisher	Cat #: M23400
Cresyl violet acetate	MP Biomedicals	Cat #: 02150727
Isoflurane	Phoenix Pharmaceuticals	N/A
Ketamine hydrochloride (VetaKet ®)	Akorn Animal Health	N/A
Xylazine (AnaSed ®)	Lloyd Laboratories	N/A
Paraformaldehyde	Alfa Aesar	Cat #: AA-A11313-22
Experimental Models: Organisms/Strains		
Sprague-Dawley Norway rats	Envigo	RRID:RGD_10401918
Software and Algorithms		
MATLAB v 2015b	Mathworks	RRID:SCR_001622
Spike2 Software	Cambridge Electronic Design	RRID:SCR_000903
SPSS Statistics	IBM	RRID:SCR_002865
BSMART toolbox	[35]	http://www.brain-smart.org/
Other		
Stereotaxic apparatus	David Kopf Instruments	Model: 900
Freezing microtome	Leica	Model: SM2000 R
Fluorescent microscope/camera	Leica	Model: DMLS/DFC300FX
Stainless steel EMG wire	California Fine Wire	Cat #: M408090
Microsyringe	Hamilton	REF: 65457-02
Cambridge Electronic Design recording system	Cambridge Electronic Design	N/A
Digital Tucker-Davis recording system	Tucker-Davis Technologies	N/A
Recording electrodes	NeuroNexus	Models: A1x16-Poly2-5mm-50-177; A1x16-10mm-100-177; Q1x4-10mm-50-177